

Wind accretion in binary stars – II. Accretion rates

Tom Theuns¹, Henri M.J. Boffin^{2,3}, Alain Jorissen^{2*}

1: Department of Physics, Nuclear Physics Laboratory, Keble Road, Oxford OX1 3RH, UK

2: Université Libre de Bruxelles, Institut d’Astronomie et d’Astrophysique, Campus Plaine CP 226, Boulevard du Triomphe, B-1050 Bruxelles

3: Present address : Department of Earth and Planetary Sciences, Kobe University, Kobe 657, Japan

17 May 2018

ABSTRACT

Smoothed particle hydrodynamics (SPH) is used to estimate accretion rates of mass, linear and angular momentum in a binary system where one component undergoes mass loss through a wind. Physical parameters are chosen such as to model the alleged binary precursors of barium stars, whose chemical peculiarities are believed to result from the accretion of the wind from a companion formerly on the asymptotic giant branch (AGB). The binary system modelled consists of a $3M_{\odot}$ AGB star (losing mass at a rate $10^{-6} M_{\odot} \text{ y}^{-1}$) and a $1.5M_{\odot}$ star on the main sequence, in a 3 AU circular orbit. Three-dimensional simulations are performed for gases with polytropic indices $\gamma = 1, 1.1$ and 1.5 , to bracket more realistic situations that would include radiative cooling. Mass accretion rates are found to depend on resolution and we estimate typical values of 1-2% for the $\gamma = 1.5$ case and 8% for the other models. The highest resolution obtained (with 400k particles) corresponds to an accretor of linear size $\approx 16R_{\odot}$. Despite being (in the $\gamma = 1.5$ case) about ten times smaller than theoretical estimates based on the Bondi-Hoyle prescription, the SPH accretion rates remain large enough to explain the pollution of barium stars. Uncertainties in the current SPH rates remain however, due to the simplified treatment of the wind acceleration mechanism, as well as to the absence of any cooling prescription and to the limited numerical resolution.

Angular momentum transfer leads to significant spin up of the accretor and can account for the rapid rotation of HD 165141, a barium star with a young white dwarf companion and a rotation rate unusually large among K giants.

In the circular orbit modelled in this paper, hydrodynamic thrust and gravitational drag almost exactly compensate and so the net transfer of linear momentum is nearly zero. For small but finite eccentricities and the chosen set of parameters, the eccentricity tends to decrease.

Key words: accretion, accretion discs – hydrodynamics – binaries : close – stars: barium

1 INTRODUCTION

Wind accretion in a binary system influences the surface composition and spin of the accreting star and can change the orbital parameters of the binary. This paper aims at estimating these effects in a binary system in which one of the components is an asymptotic giant branch (AGB) star which suffers from strong mass loss ($\dot{M} \approx 10^{-6} M_{\odot} \text{ y}^{-1}$) through a wind. The companion main sequence (MS) star accretes some of this carbon and s-process element enriched gas and mixes it in its envelope. Stellar evolution will eventually transform the AGB star into a white dwarf (WD) and

the initially less massive MS star into a chemically peculiar giant.

This is the evolutionary scenario proposed by Boffin & Jorissen (1988) for the formation of barium stars, i.e. late-type giants exhibiting overabundances in carbon and s-process elements (e.g. Lambert 1985). All barium stars are likely members of a binary system with a WD companion (McClure & Woodsworth 1990, Jorissen & Boffin 1992).

The theoretical description of the accretion process is complex due to the intricate structure of the flow and the complex non-linear hydrodynamics of the shocked wind material. One can estimate the expected fraction \dot{M}_{acc}/\dot{M} of material being accreted (Boffin & Jorissen 1988) from an interpolation formula due to Bondi & Hoyle (1944) and Bondi (1952) for the accretion rate onto a star moving at con-

* Research Associate, National Fund for Scientific Research (FNRS), Belgium

stant velocity through a gas of uniform density and temperature. This involves the interpolation of the estimated accretion rates from two even more simplified models. In the first model (Hoyle & Lyttleton 1939), one neglects gas pressure and estimates the accretion rate \dot{M}_{HL} onto a compact gravitating object with mass M , moving at constant velocity v_∞ through a pressureless medium with initially uniform density ρ_∞ . In this model, gravitationally deflected material which passed on one side of the star collides with material passing on the opposite side, thereby cancelling its transverse velocity and forming an ‘accretion line’ behind the star. The material from this accretion line that has a velocity below the local escape velocity from the star will be accreted and one finds (Hoyle & Lyttleton 1939):

$$\dot{M}_{HL} = \pi R_A^2 \rho_\infty v_\infty, \quad (1)$$

where the accretion radius R_A is given by

$$R_A = 2GM/v_\infty^2. \quad (2)$$

The second model (Bondi 1952; see also Theuns & David 1992 for the closed form solution of the flow pattern) includes gas pressure but neglects instead the motion of the star through the medium. The accretion rate in a steady state is not uniquely determined but the model does provide a maximum accretion rate \dot{M}_B :

$$\dot{M}_B = \alpha \pi R_B^2 \rho_\infty c_\infty, \quad (3)$$

where the Bondi radius is given by Eq. (2) but with the sound speed at infinity c_∞ replacing v_∞ . The efficiency parameter α is of the order of unity and depends on the value γ of the polytropic index of the gas. The accretion rate \dot{M}_{BH} for the Bondi-Hoyle case, where both the velocity of the star as well as gas pressure are included, is based on an interpolation between these two extreme cases:

$$\dot{M}_{BH} = \alpha \pi R_A^2 \rho_\infty v_\infty \left(\frac{\mathcal{M}_\infty^2}{1 + \mathcal{M}_\infty^2} \right)^{3/2}, \quad (4)$$

where $\mathcal{M}_\infty \equiv v_\infty/c_\infty$ is the Mach number.

The theoretically predicted accretion rate \dot{M}_{BH} in the Bondi-Hoyle model has been extensively tested against numerical simulations by e.g. Hunt (1971) and more recently by Ruffert (1994) and Ruffert & Arnett (1994). The theoretical and numerical rates agree to within 10% which must be considered a bit fortuitous since e.g., although transiently present, no accretion line (as envisaged in the Hoyle and Lyttleton picture) actually exists. The latter simulations also show the importance of numerical resolution on the computed accretion rates.

In a previous paper (Theuns & Jorissen 1992, Paper I), we presented three-dimensional (3D) smoothed particle hydrodynamics (SPH) simulations of wind accretion, taking into account the binary motion. Two-dimensional simulations of this problem were previously done by Sørensen et al. (1975) and by Matsuda et al. (1987, 1992). Even a glancing comparison between the structure of the flow in this case (Paper I) against that in the Bondi-Hoyle model (as in e.g. Ruffert & Arnett 1994) shows that the binary motion induces a very different flow pattern. Consequently, using the accretion rate \dot{M}_{BH} in this situation as well might be stretching one’s luck too far.

The main aim of this paper is to test whether the mass accretion rates are large enough to produce barium stars

through the wind accretion scenario discussed above. The impact of wind accretion on the orbital parameters and on the spin velocity of the accretor will also be evaluated. An especially important diagnostic of wind accretion is provided by the variation of the orbital eccentricity caused by the transfers of linear momentum between the gas and the accreting star. Moreover, if the accreted gas possesses angular momentum, the spin period of the accreting star can be altered. Several aspects considered in the present paper may also be relevant to the study of wind accretion in symbiotic stars or in ζ Aurigae systems.

In addition to the complications introduced by the binary motion, uncertainties about the thermodynamic state of the gas call for caution when deducing the accretion rate from oversimplified models. In fact, the simple polytropic equation of state adopted in this paper for the gas may not be appropriate in these systems exhibiting ‘cooling radiation’ in the form of UV light. Interacting systems such as symbiotic or extrinsic S stars, where wind accretion is currently taking place, indeed exhibit a wealth of UV emission lines or continuum UV radiation (e.g. Nussbaumer & Stenel 1987; Johnson & Ameen 1991). In the interacting S star HD 35155 for example, a total UV continuum emission of about $0.2 L_\odot$ is observed (Johnson & Ameen 1991). In Paper I, we identified regions of shocked gas as being responsible for this kind of emission.

Comparison of the accretion rates obtained for different γ ’s nevertheless allows us to appraise the importance of the assumed polytropic index on the computed rates.

2 MODELING WIND ACCRETION WITH SPH

2.1 Description of the numerical method

All numerical details can be found in Paper I. Only a short summary will be given here. Calculations are done in an inertial frame in which the motion of the centers of mass of the two stars, AGB and MS, are computed from the solution of the two-body problem for a circular orbit, neglecting all hydrodynamic effects. The hydrodynamics of the gas, on the other hand, is treated by means of variable resolution SPH (Lucy 1977; Gingold & Monaghan 1977; see e.g. Benz 1989 for a review).

Gas forces include the hydrodynamic pressure force, $\nabla p/\rho$, the gravitational force from the MS star and from the AGB star. In addition, a mechanism responsible for the AGB wind acceleration is included, simulating the effects of the AGB pulsations and radiation pressure on the escaping gas (see e.g. Bowen 1988). Since the luminosity force per unit mass falls with distance like $1/r^2$, just as the gravitational force does, one can implement such an acceleration mechanism by decreasing the effective AGB star mass where it enters the interaction with the gas. In these simulations, we assume an accelerating force which exactly balances the gravitational force from the AGB (resulting in a wind velocity independent of the distance from the mass-losing star, as obtained in Bowen’s wind models). Self-gravity of the gas is neglected.

A specific model is characterized by the orbital elements of the binary (radius A of the circular orbit and period P corresponding to a circular velocity $V_c \equiv 2\pi A/P$), the mass

ratio of the two stars and the properties of the wind, i.e. its polytropic index γ and its velocity, mass flux and sound speed at the surface of the AGB star.

In addition to these physical parameters, there are additional purely numerical parameters, most critically the effective resolution. The latter is determined by the total number of SPH particles used. We estimate this resolution by computing the average smoothing length \bar{h} (see Paper I) for particles around the accreting star. That length characterizes the size of the interpolation region over which quantities are smoothed in the SPH formalism.

The simulations are started with vacuum initial conditions. A supersonic wind is started around the AGB star and the model is integrated until a quasi steady-state is reached. The resolution is then improved by increasing the number of particles emanating from the AGB star per unit time (yet keeping the mass flux fixed). It is possible to monitor in this way how the accretion rates change as a function of resolution. The accretion process is simulated by removing mass from the flow, once it enters a sphere with radius \bar{h} around the accreting star. The average resolution \bar{h} is computed from all particles in a sphere of radius r_h around the accreting star.

2.2 Calculation of fluxes

Accretion rates are computed by measuring fluxes round the secondary. Two different methods are used to compute fluxes (see also Paper I). The flux $\Phi_{\mathcal{A}}$ of a quantity \mathcal{A} is defined by

$$\Phi_{\mathcal{A}} = - \int_{\Sigma} \mathcal{A} \rho \mathbf{v} \cdot d\mathbf{S}, \quad (5)$$

where ρ and \mathbf{v} denote the fluid density and velocity respectively, $d\mathbf{S}$ is the outward surface element of a sphere with radius R centered on the accreting star. In the first method for evaluating fluxes, the flux density $\mathcal{A} \rho \mathbf{v}$ entering Eq. (5) has been evaluated using its SPH estimate on 20×20 points uniformly spaced in $\cos \theta$ and ϕ on the surface of the sphere of radius R (with θ and ϕ being the usual spherical coordinates with respect to the centre of the sphere). A numerical integration over the surface of the sphere then gives $\Phi_{\mathcal{A}}$.

Alternatively, $\Phi_{\mathcal{A}}$ can be computed by summing over SPH particles of mass m_i :

$$\Phi_{\mathcal{A}} = \sum_i \frac{dm_i}{dt} \mathcal{A}_i. \quad (6)$$

For $\mathcal{A} = 1$, $\Phi_{\mathcal{A}}$ represents the mass accretion rate. In that case, $\Phi_{\mathcal{A}}$ should be independent of R for a stationary flow (as long as the sphere does not reach other sources or sinks, like e.g. the mass-losing star or the outer boundary). The comparison of the mass accretion rates computed from the flux through spheres of different radii thus provides a way of evaluating the stationarity of the flow (see Fig. 3). For $\mathcal{A} = v_x$, $\Phi_{\mathcal{A}}$ represents the momentum accreted in the x -direction. In that case, $\Phi_{\mathcal{A}}$ does depend on R , since the velocity v_x of a fluid particle changes due to the gravitational force of the accreting star. However, the total force on the star, which is the sum of the accreted momentum and the gravitational force exerted by the gas on the star, should again be independent of R . Finally, for $\mathcal{A} = xv_y - yv_x$, $\Phi_{\mathcal{A}}$ is the accreted spin momentum.

2.3 Test simulations

We tested our code and the prescription for calculating fluxes by simulating Bondi accretion, i.e. the spherically symmetric accretion of polytropic gas onto an accretor of constant mass M (Sect. 1) at rest. Given the sound speed c_{∞} and density ρ_{∞} of the gas at infinity, this problem has a family of solutions which differ by the effective accretion rate. The so-called transonic branch corresponds to the situation where the flow changes from subsonic at large distances to supersonic close to the accreting object. This solution has the largest accretion rate (e.g. Theuns & David 1992). A flow pattern corresponding to this branch and matching the analytical solution is first set up. The parameters M , c_{∞} and ρ_{∞} are then scaled in order to get flows with the same average resolution \bar{h} within the sphere of radius r_h , but with the sonic point falling either outside the accreting sphere's surface (the 'supersonic' model) or inside the accreting sphere (the 'subsonic' model). Note that the *physical model* is identical in both cases, the only difference being in the place where mass is removed from the flow: in the subsonic model, potentially all mass is removed from the flow before it has managed to become supersonic.

The upper panel of Fig. 1 compares the simulation results for the 'subsonic' case with the analytical solution. The agreement is satisfactory outside the accreting sphere (only there is the comparison meaningful, obviously). The deduced accretion rates in the stationary regime are 20% low with respect to the analytic value (lower panel of Fig. 1), which is sufficient for our purpose. The agreement is better in case the sonic point falls outside the accreting sphere (the 'supersonic' model). Note that the difference between analytic solution and simulation is likely to be due, not only to the accuracy of the flux calculation itself, but also to how well the initial profile matches the analytic profile. The resolution in these test cases, in terms of the number of particles inside the region in which particles are being accreted, is comparable to the resolution obtained in the standard wind accretion case, to be discussed in Sect. 2.4.

2.4 Numerical simulations

All the simulations considered in this paper are for a binary system consisting of a $3 M_{\odot}$ AGB star and a $1.5 M_{\odot}$ companion in a circular orbit around the AGB star with a semi-major axis of 3 AU (corresponding to a period of 895 d, and an orbital velocity of 36 km s^{-1}). The AGB star is losing mass at a steady rate of $\dot{M}_1 = 10^{-6} M_{\odot} \text{ y}^{-1}$ with a (constant) wind velocity of 15 km s^{-1} (here, and in what follows, subscripts 1 will refer to the mass-losing star). The sound speed at the base of the flow is 7.6 km s^{-1} (corresponding to a temperature of about $4050/\gamma \text{ K}$ at the surface of the AGB star; note that this sound speed is larger than the value used in Paper I). Three models are considered which differ only in the assumed value of γ (1.5, 1.1 and 1). Unless stated otherwise, we use units in which period P , semi-major axis A and gravitational constant are all unity. In these units, the parameter r_h (Sect. 2.1) is taken equal to 0.3.

Table 1 provides the conditions for the different runs performed and the corresponding accretion rates. The successive columns give the total number of particles N , the polytropic index γ , the average resolution $2\bar{h}$ inside the

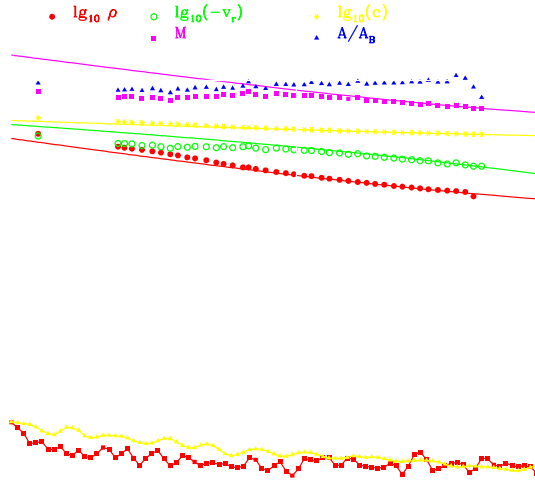


Figure 1. Comparison of SPH test simulation (with $\gamma = 1.5$) against analytic solution for the transonic branch of Bondi accretion. The corresponding Bondi radius, as defined in Eq.(3), is 400 in our units. Upper panel: SPH profiles (in the stationary regime) of density ρ , infall velocity v_r , sound speed c , mass flux $A = -4\pi r^2 \rho v_r$ (normalised by the analytical value A_B) and Mach number \mathcal{M} compared with the analytic solution (solid lines). For the sake of clarity, density, velocity and sound speed profiles have been offset by -1, -0.7 and -0.4, respectively. Particles to the left of the vertical line are used to compute the average resolution \bar{h} around the accreting object (i.e. $\log_{10}(r_h) = 0.9$).

Lower panel: accretion rates (normalised to the analytical value) determined from Eq. (6) (curve labelled ‘acc’) compared with rates determined from Eq. (5) for three values of the radius R ($R = 2\bar{h}$, labelled ‘g2’; $R = 3\bar{h}$, labelled ‘g3’; $R = 4\bar{h}$, labelled ‘g4’, where $\bar{h} \approx 0.8$), as a function of time. For times ≥ 2 , a steady-state is reached.

Table 1. Basic data and accretion rates for the different cases considered

N	γ	$2\bar{h}/A$	$2\bar{h}$ R_\odot	t/P	\dot{M}_2/\dot{M}_1 %	H_y $\dot{M}_2 V_c$	G_y $\dot{M}_2 V_c$	F_y $\dot{M}_2 V_c$	$\dot{L}_z/V_c A \dot{M}_2$
100k	1.5	0.11	71	24	2	-1.5	1.55	0.05	0.06
100k	1.1	0.10	64	17	8	–	–	–	0.06
70k	1	0.10	64	22	8	–	–	–	0.06

sphere of radius r_h around the accreting star [as is common practice, we use $2\bar{h}$ to characterise the resolution because the SPH kernel $W(r/h)$ becomes zero for $r > 2h$, see Paper I], expressed relative to the orbital separation and in solar radii, the number of orbital periods during which the simulation has been carried out (t/P), the fraction of the mass lost by the AGB star that is accreted by the companion (\dot{M}_2/\dot{M}_1), the hydrodynamic, gravitational and total drags (H_y , G_y and F_y , respectively, expressed in terms of the accreted momentum $\dot{M}_2 V_c$), and finally the dimensionless spin accretion rate $\dot{L}_z/V_c A \dot{M}_2$. The various accretion rates will be described in more details in Sect. 3.1. A dash in Table 1 means that the value has not been computed.

Each simulation typically requires about two weeks of CPU time on a HP-730 workstation. In terms of the accretion radius R_A [Eq.(2)], the resolution achieved around the accreting star amounts to $2\bar{h}/R_A \sim 0.2$, since $R_A = 380 R_\odot$. Since this resolution is much higher than in Paper I (100k particles instead of 40k particles for the case $\gamma = 1.5$), Fig. 2 displays a general view of the flow pattern, as well as a zoom on the region close to the accreting star. Despite a larger sound speed at the surface of the AGB star, the general

structure of the flow is similar to that described in Paper I. It is worth noting in relation with the discussion of Sect. 5.1 that the Roche-lobe geometry is not at all apparent in the flow structure, because the wind acceleration mechanism has the net effect of suppressing the gravitational potential of the AGB star (see Sect. 2.1).

3 RESULTS

3.1 SPH accretion rates

The accretion rates of mass, momentum and spin for the three values of the polytropic index ($\gamma = 1, 1.1$ and 1.5) considered in this paper are given in Table 1. They will be discussed in some detail here for the $\gamma = 1.5$ (adiabatic) case only, since the same remarks apply to the other cases as well.

Figure 3 shows the accretion rates as a function of time. The top panel indicates that the two methods of determining the fluxes, namely direct summation over SPH particles (Eq. 6) or estimates of SPH fluxes (Eq. 5), give very similar results: about 2 to 2.5% of the mass lost by the AGB star is

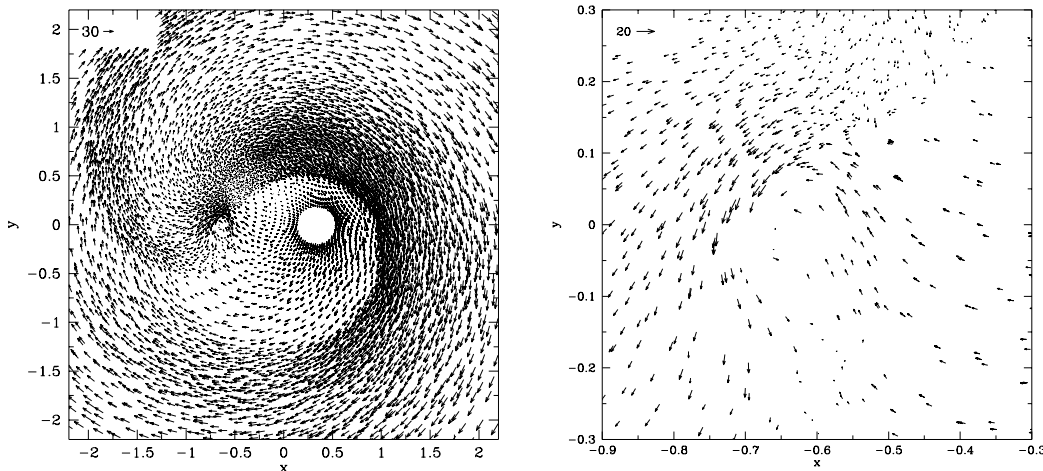


Figure 2. Left panel: General structure of the velocity field in the orbital plane for the adiabatic case $\gamma = 1.5$ with 100k particles. Only particles lying in a z -slice $[-0.1, 0.1]$ enclosing the orbital plane are represented. The stationary frame in which the mass-losing star is at $(x = 0.33, y = 0, z = 0)$ and the accreting star at $(x = -0.66, y = 0, z = 0)$ has been used. Right panel: Same as left panel, zoomed in on the accreting star. The spin momentum carried by the wind close to the accretor is apparent.

accreted by the companion (but see below). Incidentally, the fact that the mass fluxes through spheres of different radii are almost equal indicates that the flow pattern is relatively stationary.

The middle panel gives the forces exerted by the gas on the accreting star, due to the accretion of linear momentum (hydrodynamic drag, labeled H) and due to the gravitational pull of the gas lagging behind the accretor (labeled G). More precisely, the accretion of linear momentum has been computed from

$$\mathbf{H} = \mathbf{P} - \dot{M}_2 \mathbf{v}_2, \quad (7)$$

where $\mathbf{P} \equiv \sum_w \mathbf{v}_w \partial m_w / \partial t$ denotes the momentum in the wind, accreted by the star. The index w indicates that the sum extends over SPH particles. The inertial forces in this figure are projected on a set of axes, with the x axis along the line joining the two stars, the mass-losing star lying on the $+x$ axis with its orbital motion pointing along $+y$, and finally the z axis being perpendicular to the orbital plane. The gravitational drag G , on the other hand, is computed by summing over SPH particles in the wind as:

$$\mathbf{G} = \sum_w \mathbf{F}_{grav,w}. \quad (8)$$

The net force acting on the star is labeled $F \equiv G + H$.

The hydrodynamic drag is negative, for both radial and tangential directions. This means that the accreting star is propelled away from its companion and is accelerated along its orbit due to the gas raining back onto it from $y > 0$ (i.e., a thrust rather than a drag), as apparent from Fig. 2. However, the gravitational forces have exactly the opposite

tendency and the net effect is an inward pull and a very slight slowing down of the star along its orbit.

The bottom panel shows the accretion of the dimensionless spin angular momentum, again obtained by summing over SPH particles:

$$\frac{\dot{\mathbf{L}}}{A V_c M_2} = \sum_w (\mathbf{r}_w - \mathbf{r}_2) \times (\mathbf{v}_w - \mathbf{v}_2) \frac{1}{A V_c M_2} \frac{\partial m_w}{\partial t} \quad (9)$$

The radial (x) and tangential (y) components fluctuate around zero, as expected from the symmetry of the flow along the z direction (perpendicular to the orbital plane). There is, however, a net accretion of spin momentum in the z direction, in such a way that the accreting star tends to be spun up if it is in synchronous rotation to begin with. This can be clearly seen on Fig. 2 from the direction of rotation of the disc-like structure around the accreting star. The accretion rates of dimensionless spin momentum are remarkably similar amongst the three models, notwithstanding the fact that a much better-developed accretion disc forms in the isothermal case (compare Figs. 1 and 8 of Paper I).

We tried to improve our estimate of M_2/M_1 by increasing the resolution drastically in a small region around the accreting star. However, conclusions drawn from simulations involving such a restricted region will be meaningless once boundary effects propagating inwards become important. In order to illustrate that effect, a simulation has been performed with most of the particles removed, except for those close to the accreting star. As illustrated by Fig. 4, the accretion rate does not change when measured over a sufficiently short interval of time, but starts deviating when boundary effects propagate into the accretion sphere

(round $t/P = 24.34$). In Fig. 4, the line labeled ‘large box’ corresponds to the accretion rate for the standard model[†], whereas the dotted line, labeled ‘small box’, includes particles close to the accreting star only (in fact, the small box *with the same* resolution as the large box, contains only 4% of the number of particles of the large box). Obviously, for $t/P \leq 24.34$, the accretion rates remain identical yet start to diverge afterwards. Therefore, the high-resolution simulations described below, and involving the small box, are only meaningful for $t/P \leq 24.34$. In order to artificially increase the resolution, we proceed as follows. At time $t/P = 24.30$, each SPH particle is replaced by a swarm of n particles, distributed around their mother according to the SPH density kernel. This increases the resolution by a factor $n^{1/3}$. The different curves in Fig. 4 correspond to simulations with $n = 1$ (dotted), $n = 10$ (triangles), $n = 25$ (dots) and $n = 90$ (squares), which translates into a number of particles in the small box around the accreting star of $4k$, $40k$, $100k$ and $360k$, respectively. Drawing conclusions from these numerical experiments is hampered by the fact that the accretion rate varies quite considerably over time intervals of the order of $0.02P$, as is clear from the $n = 1$ case (solid line). These variations on a time scale much longer than the time step $\delta t \leq 5 \times 10^{-4}P$ simply reflect the discrete episodes of particle ejections by the mass-losing star (see Sect 2.3 of Paper I). In addition, once SPH particles are cloned, as described above, the system needs some time to relax to a new steady state. The following conclusions can nevertheless be drawn from these simulations: 1) the accretion rate *decreases* with increasing resolution, and 2) the mass accretion rate is not likely to be much less than about 1%, i.e. about 1/3 lower than deduced from the standard model. This value follows assuming that the almost linear trend observed in Fig. 5, which displays numerical resolution versus mass accretion rate, can be extrapolated to the size of a main sequence accretor (i.e., $2\bar{h} \approx 1.5 \times 10^{-3}$ which corresponds to $1R_{\odot}$). In what follows we will use an estimated mass accretion rate of 1% for the adiabatic model, but we stress that an accurate estimate of the real accretion rate requires much higher resolution simulations than the ones presented here.

3.2 Comparison with the Bondi-Hoyle mass accretion rate

In Sect. 3.1, a mass accretion rate $\beta = -dM_2/dM_1$ of the order 1% is derived from our SPH simulations in the $\gamma = 1.5$ case. That result will now be compared to the accretion rate derived by the Bondi & Hoyle (1944) formula. In the framework of a binary system, the gas velocity v_{∞} appearing in Eq. (4) may be replaced by the relative velocity between the wind and the accreting star, whereas the gas density ρ_{∞} may be replaced by the wind density ρ at the location of the accreting star. The latter may be deduced from the mass conservation equation $\dot{M}_1 = -4\pi r^2 v_w \rho$. Substituting these expressions into Eq. (4) yields

[†] The reason why the standard case yields accretion rates of the order of 2.5–3.5% in Fig. 4 as compared to 2.0–2.5% in Fig. 3 is because the latter correspond to time averages.

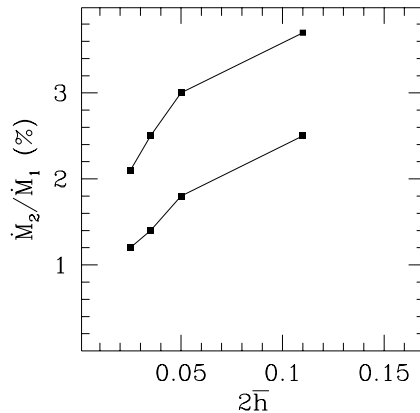


Figure 5. Accretion rates of mass (M_2/\dot{M}_1 , in %) as a function of resolution, $2\bar{h}$, for the $\gamma = 1.5$ model. The upper and lower curves correspond to the maximum and minimum accretion rates for these resolutions, read from Fig. 4.

$$\beta = \frac{\alpha}{A^2} \left(\frac{GM_2}{v_w^2} \right)^2 \frac{1}{[1 + (v_{\text{orb}}/v_w)^2 + (c/v_w)^2]^{3/2}}, \quad (10)$$

or using Kepler’s third law:

$$\beta = \alpha \mu^2 \frac{k^4}{[1 + k^2 + (c/v_w)^2]^{1.5}}, \quad (11)$$

where α is a parameter of order unity not fixed by the theory, $\mu \equiv M_2/(M_1 + M_2)$, $k \equiv v_{\text{orb}}/v_w$, and v_{orb} is the orbital velocity.

For the conditions given in Sect. 2.4, Eq. (11) yields $\beta \simeq 10$ to 20% for $k = 2.4$, taking α between 0.5 and 1, as suggested by the numerical simulations of Ruffert & Arnett (1994). The accretion rate deduced from the SPH simulation in the $\gamma = 1.5$ case is thus about ten times smaller than that predicted by the Bondi & Hoyle formula. The reason for this apparent discrepancy is that Eq. (11) is only applicable to situations where $k \ll 1$, since it was originally derived by considering a single star moving through a gas cloud. In the case of a fast wind ($k \ll 1$), the concept of accretion column as introduced originally by Bondi & Hoyle to describe the accretion process, does hold with the accretion column being tilted with respect to the radius vector. When k is of the order of unity, however, as is the case here, the binary motion strongly disturbs the shape of the accretion column, as is obvious from Fig. 2. The fact that the above formula becomes meaningless for large values of k is further illustrated by the fact that β increases like k when $k \gg 1$, though values of β larger than unity have of course no physical meaning. The fact that the Bondi-Hoyle formula Eq. (11) was not expected to hold in the case of accretion of a slow wind was the prime motivation to perform the simulations described here.

Finally, note that the term $(c/v_w)^2$ in Eq. (11) is usually negligible (in the case of adiabatic wind expansion, c decreases as $r^{-(\gamma-1)}$), and has therefore not been considered in the above discussion.

4 CONSEQUENCES OF WIND ACCRETION

Wind accretion can alter the evolution of a binary in several respects:

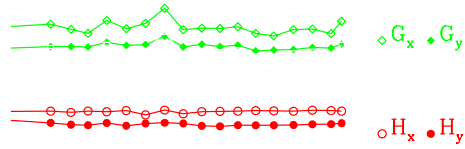


Figure 3. Accretion rates as a function of time for the $\gamma = 1.5$ case.

Top panel: accretion rates of mass (\dot{M}_2/\dot{M}_1 , in %). The different symbols represent estimates based on Eq. (6) (filled dots, labeled ‘acc’) or on Eq. (5) with three different radii R (0.11, 0.16 and 0.22, labeled ‘g2’, ‘g3’ and ‘g4’, respectively).

Middle panel: accretion rates of linear momentum in the radial (subscript x) and tangential (y) directions, in units of $\dot{M}_2 V_c$: H refers to the hydrodynamic drag, G to the gravitational drag and F to the sum of those (see text for details).

Bottom panel: rate of accretion of dimensionless spin momentum, $\dot{L}/\dot{M}_2 V_c A$, in the radial x , tangential y and z directions. Spin momenta along x and y are multiplied by ten.

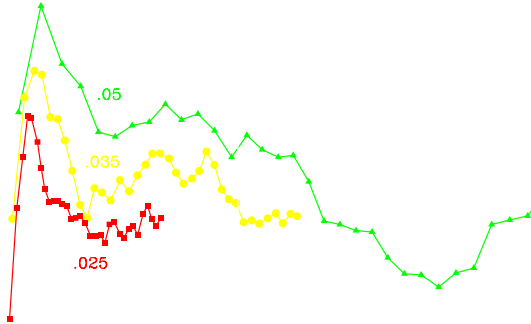


Figure 4. Accretion rates of mass (\dot{M}_2/\dot{M}_1 , in %) as a function of time (in units of the orbital period P) for the $\gamma = 1.5$ model with different resolutions $2\bar{h}$. The solid curve labeled ‘large box’ refers to the standard model. The dotted line labeled ‘small box’ corresponds to a simulation where only those particles close to the accretor are retained. Up to $t/P \approx 24.34$, these two rates are identical. The other curves (triangles, dots and squares) refer to simulations in a ‘small box’ as above, but with an initial number of particles increased as indicated in the text. The different curves are labeled with their effective resolutions.

- the chemical composition of the envelope of the accreting star may be modified if the accreted matter has a different composition, and if enough such mass is accreted;
- the orbital elements may change as a result of the mass loss and mass transfer;
- the accreting star may be spun up if the accreted matter possesses significant angular momentum.

Each of these effects is now considered in turn on general grounds. Application to barium stars will be considered in Sect. 5.

4.1 Envelope pollution

The pollution of the envelope of the accreting star depends on (i) the amount of mass ΔM_2 accreted from the wind, (ii) the dilution factor of the accreted matter in the envelope, and (iii) the extent to which the chemical composition of the accreted matter differs from that of the envelope. We will assume that the accreted matter has been fully mixed in the envelope. In the case that the accreting star is on the giant branch, such a mixing naturally results from the convective nature of the envelope. In the other case where the accreting star is still on the main sequence, some mixing will occur if the accreted matter has a mean molecular weight larger than that of the underlying layers (Proffitt 1989; Proffitt & Michaud 1989). Such an inversion of mean molecular weight, triggering a turbulent mixing until the inversion is suppressed, is expected if carbon-rich matter from the wind of an AGB star falls on top of the surface layers of the main sequence star.

The overabundance f_i of element i in the envelope of the accreting star (i.e. the ratio between the abundance after completion of the accretion and mixing processes, and the abundance in the primordial envelope) is related to its overabundance g_i in the wind (i.e. in the AGB atmosphere) through the relation

$$f_i = \frac{g_i \Delta M_2 + M_{2,0} - M_{2,\text{core}}}{\Delta M_2 + M_{2,0} - M_{2,\text{core}}} \equiv g_i \mathcal{F} + (1 - \mathcal{F}), \quad (12)$$

where \mathcal{F} is the dilution factor of the accreted matter ΔM_2 in the envelope of mass $(M_2 - M_{2,\text{core}})$. Here, $M_{2,0}$ and $M_{2,\text{core}}$ denote the total initial and core mass, respectively, of the accreting star. In deriving the above relation, it has been assumed that gas and grains are accreted with the same efficiency. The chemical fractionation that occurs between the gas and grain phases in the AGB wind (due to the different refractory properties of the different chemical elements) is then erased once they mix again in the companion's envelope. This assumption is actually not always satisfied: in some observed post-AGB star binaries only gas and no grains have been accreted (e.g. Waters et al. 1992).

4.2 Variation of orbital parameters

The orbital parameters of the binary will change as a consequence of the mass lost from the system, the mass transferred from one star to the other, the gravitational force of the wind on both stars and finally, the change in momentum of the accretor, due to the accretion of momentum from the wind. In addition, the mass loss process itself may be asymmetric, providing an extra source of momentum changing

the orbital parameters, but that possibility will not be considered here.

Huang (1956) derives expressions for such changes in an adiabatic approximation, i.e., when the change per period is small. However, Huang's parametrization does not allow to compare the respective effects of drag and mass accretion on the variations of the orbital elements, though the former effect is of importance in the situation modelled in this paper (as can be judged from Fig. 3). Therefore, Eqs. (13 – 15) describing the variation of the orbital elements are parametrized in term of F_y , the tangential component (i.e. perpendicular to the radius-vector, and positive along the orbital motion of the mass-losing star 1) of the total force, including gravity and accretion of linear momentum. With the notations of Sect. 3.1, $F_y = G_{2,y} - (M_2/M_1)G_{1,y} + H_y$, as displayed in Fig. 3 (but note that we neglected the gravitational force $G_{1,y}$ exerted by the gas on the mass-losing star in that figure). That quantity, as well as the mass accretion rate, are assumed to remain constant during one orbital cycle: this is probably a good approximation as long as $e \ll 1$ (e is the eccentricity of the orbit). Following this line of argument (see the Appendix for more details), we find, neglecting all terms of order e^2 or higher:

$$\frac{\dot{A}}{A} = -\frac{\dot{M}_1 + \dot{M}_2}{M_1 + M_2} - 2\frac{F_y}{M_2 V_c} \quad (13)$$

$$\frac{\dot{P}}{P} = -2\frac{\dot{M}_1 + \dot{M}_2}{M_1 + M_2} - 3\frac{F_y}{M_2 V_c} \quad (14)$$

$$\frac{\dot{e}}{e} = -\frac{1}{2}\frac{\dot{M}_2}{M_2} + \frac{3}{2}\frac{F_y}{M_2 V_c}. \quad (15)$$

Equations (13) and (14) illustrate basically the same physical effects: mass loss from the system ($\dot{M}_1 + \dot{M}_2 < 0$) increases A and P (first term), and slowing down of the accretor or speeding up of the mass-loser due to the exerted forces ($F_y > 0$) has the opposite effect (last term). The behaviour of the eccentricity can be written slightly more revealing in the case of equal masses:

$$\frac{\dot{e}}{e} = \frac{3}{2}\left(\frac{1}{6} + \frac{v_{w,y}}{V_c}\right)\frac{\dot{M}_2}{M_2} + \frac{3}{2}\frac{G_{2,y} - G_{1,y}}{M_2 V_c}, \quad (16)$$

(for $M_1 = M_2$)

where $v_{w,y}$ is the tangential wind velocity, at the point it is accreted. (We have replaced $v_{2,y}$ by $-V_c/2$ in doing this transformation, which is a valid approximation since the eccentricity is assumed to be small.) Obviously, if the orbit is circular to begin with, it stays circular. Next, in the absence of accretion ($\dot{M}_2 = 0$), the eccentricity will *increase*, since most of the wind material is lagging behind star 2 ($G_{2,y} > G_{1,y} > 0$), as can be seen on Fig. 1b of Paper I. Hence the second term is positive. Finally it will depend on the value of the accretion rate \dot{M}_2 and the wind velocity at the point it is accreted, whether e will increase (second term dominates) or decrease (first term dominates).

Applying Eq. (15) to our case, we find that the eccentricity *decreases* for our set of parameters (see Fig. 3), its relative variation being of the order of $-\partial M_2/M_2$, i.e. a few percent only. Including the gravitational force due to the gas on the mass-losing star strengthens this conclusion.

4.3 Influence on spin

The companion star may accrete spin angular momentum from the wind, which may alter its rotational velocity. Packett (1981) showed that a star needs to accrete only a few percent of its own mass from a keplerian accretion disc to be spun up to the equatorial centrifugal limit, essentially because stellar moments of inertia are generally much smaller than MR^2 . Less drastic effects than centrifugal breakup could already be detectable on a statistical basis by comparing the rotational velocities of post-mass transfer stars with those of single stars of the same age, thus suggesting a further observable diagnostic of mass transfer.

The initial spin angular momentum $S_{2,0}$ of the star is defined in terms of its moment of inertia $I_{2,0}$ through

$$S_{2,0} = I_{2,0} \omega_{2,0} \quad (17)$$

$$I_2 = M_2 r_g^2 R_2^2, \quad (18)$$

where $I_{2,0}$ is the initial value of I_2 . The dimensionless quantity r_g is the gyration radius. The initial spin velocity of the star is related to its initial rotational velocity through $\omega_{2,0} = v_{\text{rot},0}/R_2$, with R_2 the stellar radius. The accretion of angular momentum ΔL will change the angular velocity from $\omega_{2,0}$ to $\omega_2 = (S_{2,0} + \Delta L)(M_{2,0} + \Delta M_2)^{-1} r_g^{-2} R_2^{-2}$, assuming that r_g and R_2 did not change much as a result of the accretion process. This value should not exceed the critical centrifugal angular velocity $\omega_{\text{cr}} = [G(M_2 + \Delta M_2)/R_2^3]^{1/2}$, with G the gravitational constant. In terms of the accreted spin momentum $\Delta L \Delta M_2^{-1} A^{-1} V_c^{-1}$ as defined in Sect. 3.1, the rotation velocity v_{rot} after spin accretion writes

$$v_{\text{rot}} = (v_{\text{rot},0} + \frac{\Delta L}{\Delta M_2 A V_c} \frac{A}{R_2} \frac{1}{r_g^2} \frac{\Delta M_2}{M_{2,0}} V_c) / (1 + \frac{\Delta M_2}{M_{2,0}}). \quad (19)$$

The above equation implicitly assumes that the accreted spin has been redistributed over the entire envelope, which is equivalent to assuming that the accreted matter has been fully mixed in the convective envelope.

5 BARIUM STARS

Though the simulations described in this paper could be applied to a variety of binary systems, they were aimed at gaining some insight in the origin of barium stars. In particular they aim at checking the validity of the wind accretion model for the formation of barium stars developed by Boffin & Jorissen (1988). The impact of our hydrodynamic results on the validity of that scenario will therefore be briefly discussed in this section.

In order to evaluate the total variation of the orbital elements due to the wind accretion process, Eqs. (13)–(15) have to be integrated with M_1 as the independent variable until the mass of the AGB primary has been reduced from its initial value $M_{1,0}$ to that of its WD descendant. The total amount of mass lost by the primary during its evolution from AGB to WD, ΔM_1 , can be derived from the initial – final mass relationship. According to Weidemann (1984), a star of initial mass $M_{1,0}$ will give rise to a WD of mass M_1^{WD} , such that

$$M_1^{\text{WD}} = 0.528 - 0.044 M_{1,0} + 0.016 M_{1,0}^2. \quad (20)$$

It is assumed that this relation, derived for single WD's,

holds true as well for WD's in *detached* binary systems where mass loss occurred through a wind.

To obtain changes in composition and changes in orbital parameters, we start with $M_1 = M_{1,0}$ and integrate Eqs. (11), (13), (14) and (15) to find M_2 , A , P and e . The integration is stopped when the mass-losing star reaches its WD mass. The total amount of mass accreted by the barium star, ΔM_2 , can then be used to predict the dilution factor \mathcal{F} appearing in Eq. (12) and, hence, the pollution of the barium star envelope.

5.1 Mass accretion rate

The major result of the present paper is that the mass accretion rate obtained from our SPH simulations is significantly lower than the commonly used Bondi-Hoyle value. The extent to which such a reduction affects the ability of the wind accretion scenario to account for the chemical peculiarities of barium stars is now discussed.

As a first order approximation we assume that the accretion efficiency remains the same during the whole AGB mass loss episode, i.e. $\beta = 0.01$ (as discussed in Sect. 3.1) throughout. In that case, of the $\sim 2.45 M_\odot$ lost by the $3 M_\odot$ AGB primary [see Eq. (20)], $0.02 M_\odot$ will be accreted by the companion. This enriched material will be diluted in a $\sim 1.1 M_\odot$ envelope (i.e. adopting $0.4 M_\odot$ for the core mass), yielding a dilution factor $\mathcal{F} = 0.02$. Assuming typical heavy-element overabundances of the order of $g = 100$ in the AGB wind (e.g. Utsumi 1985), we find a final overabundance $\log_{10} f = 0.5$ dex from Eq. (12), quite a typical overabundance factor for barium stars (see e.g. Lambert 1985). In the following, dilution factors \mathcal{F} will always be converted into overabundances f by means of Eq. (12) and adopting $g = 100$ and $M_{2,\text{core}} = 0.4 M_\odot$.

The accretion efficiency β will probably not remain constant during the wind accretion process, since it very likely depends upon the orbital separation (through the ratio k of orbital to wind velocity) and upon the masses of the two stars, as suggested by Eq. (11) derived in the framework of the Bondi-Hoyle theory. It is therefore necessary to take into account the variations of the parameters k and μ resulting from the dynamics of the mass transfer process, as outlined in Sect. 3.2. Unfortunately, the small number of SPH simulations performed prevents us from checking the functional dependence between β , k and μ suggested by Eq. (11). Consequently, we are restricted to use Eq. (11), yet we normalize it in such a way as to yield our SPH result $\beta = 0.01$ when $v_w = 15 \text{ km s}^{-1}$, $A = 3 \text{ AU}$, $M_1 = 3 M_\odot$ and $M_2 = 1.5 M_\odot$.

Starting with the initial parameters as listed above, the average β over the whole mass transfer process is found to be 0.011, i.e., slightly larger than in the first order approximation where orbital parameters are kept constant (which is equivalent to fixing β at its initial value of 0.010). In other words, the accretion rate *increases* as the system widens due to the mass lost from it. This may seem rather counter-intuitive at first, but is easily derived from Eq. (10) provided that $v_{\text{wind}} \ll v_{\text{orb}}$: $\beta \propto A^{-2} v_{\text{orb}}^{-3} \propto A^{-1/2} (M_1 + M_2)^{-3/2}$ making use of Kepler's third law, and finally $\beta \propto A$ since Eq. (13) predicts $A \propto (M_1 + M_2)^{-1}$ during mass transfer when drag effects are negligible. Note that this behaviour holds as long as the wind velocity is negligible with respect to the orbital velocity.

For wide binaries, smaller β values prevail, since one can now neglect the orbital velocity with respect to the wind velocity to find that β scales as $1/A^2$ according to Eq. (10). It is therefore expected that wind accretion will be less efficient in wider systems. The sensitivity upon k predicted by Eq. (11) appears to be rather small, however, since it predicts average β values of 0.011, 0.009 and 0.007 for initial orbital separations of 3, 4 and 5 AU, respectively, all other parameters being as listed above. A substantial pollution of the companion's envelope will still result from these values of β , since the corresponding dilution factors $\mathcal{F} = 0.023$, 0.018 and 0.014, respectively, yield $\log_{10} f = 0.52$, 0.44 and 0.38 dex.

The threshold for producing a barium star in a binary system may be set to $\mathcal{F} \geq 0.005$, yielding overabundances $\log_{10} f \geq 0.17$ dex, according to Eq. (12). Below this value, the weakly polluted star would no longer be flagged as a barium star. With our new SPH scaling of Eq. (10), we find that the dilution factor \mathcal{F} drops below 0.005 for systems with final orbital periods in excess of 90 y (adopting the same parameters as above, except for the initial separation). The barium star with the longest known orbital period, ζ Cygni ($P = 17.8$ y, Griffin 1991), exhibits an average overabundance of heavy elements amounting to 0.4 dex (Začs 1994). Such an overabundance can easily be accounted for with the above prescriptions, which predict $\mathcal{F} = 0.016$ and $\log_{10} f = 0.4$ dex as required.

We conclude that the reduction in the wind accretion efficiency derived from our detailed SPH simulations when compared to the Bondi-Hoyle prescription does not endanger the validity of the wind accretion scenario. In particular we find that wind accretion can easily account for the level of pollution in barium stars with orbital periods as long as 90 y. In fact, Boffin & Začs (1994) already suggested that a reduction of the accretion rate by a factor of ten with respect to the Bondi-Hoyle value improves the agreement of wind accretion predictions with observed levels of enrichment in barium stars.

However, that scenario faces serious difficulties for systems with *short* orbital periods, albeit on different grounds. Indeed, barium systems with orbital periods of a few hundred days could not stay detached when the primary star evolved up the AGB. Standard prescriptions for AGB evolution (e.g. Groenewegen & de Jong 1993) indicate that the mass-losing star will overflow its Roche lobe at some point during its AGB evolution in systems with $P \leq 3000$ d. Since the star has a deep convective envelope at that stage, the severe mass loss due to the Roche lobe overflow (RLOF) will cause its radius to expand. But the Roche lobe tends to shrink as a result of mass transfer from the more massive to the less massive component, thus leading to a runaway behaviour of the mass transfer process. A common envelope surrounding both stars is expected to result from this process, and the drag exerted by the envelope on the binary motion will cause a severe loss of orbital energy. Binary systems with very short orbital periods (a few hours), like e.g. cataclysmic variables, are formed in such a way (e.g. Meyer & Meyer-Hofmeister 1979). Barium systems with periods of a few hundred days must somehow have escaped this dramatic fate, though these systems are not wide enough to prevent an episode of RLOF. The problem of the short period barium systems has been illustrated by the recent anal-

ysis of HD 121447 (Jorissen et al. 1995a), the barium star with the shortest orbital period (185 d). Possible solutions are investigated by Han et al. (1995).

5.2 Momentum accretion

Boffin et al. (1993) compared orbital elements of barium stars against those of normal G-K giants. They concluded that the $(e, \log P)$ diagram of barium stars could be reproduced by translating to larger periods the points representing normal giants. An increase of the orbital period is easily explained by mass loss from the system [see Eq. (13)], but the change in eccentricity depends on both the accretion rate and the influence of the gravitational and hydrodynamic forces [Eq. (15)]. Unfortunately, the latter equation is probably only valid for nearly circular orbits (for which we find a small decrease in eccentricity). Hence, we cannot draw definite conclusions about de/dt for systems which start with a finite eccentricity. In addition we caution that it is very unlikely that the barium stars with the shortest orbital periods result from the widening of systems with even shorter periods, in view of the difficulties raised by RLOF (see Sect. 5.1).

5.3 Spin accretion

The mild barium star HD 165141 possibly bears the signature of spin up due to angular momentum accretion during the mass transfer process (see Jorissen et al. 1995b for a detailed discussion of that system). HD 165141 is a K0III Ba1 star rotating much faster ($v \sin i = 14$ km s⁻¹) than normal K giants or barium stars. As shown by de Medeiros, Mayor & Simon (1992), the $v \sin i$ distribution of normal (single) K giants peaks at very low values ($v \sin i < 1$ km s⁻¹) and decreases rapidly with increasing $v \sin i$. The median of this distribution amounts to 2 km s⁻¹, with 97% of the stars having $v \sin i < 10$ km s⁻¹.

The rapid rotation of HD 165141 probably accounts for the unusually high level of chromospheric activity exhibited by that star as compared to other barium systems (CaII and CIV $\lambda 1550$ emission, relatively hard X-rays detected by ROSAT). Actually, the system has typical features of a RS CVn system, except for the long orbital period of 5200 d. This long orbital period makes it very likely that wind accretion rather than RLOF is responsible for the chemical peculiarities of this barium star. Our predictions for spin accretion presented in Sect. 4.3 may thus be applied to the HD 165141 system, which is too wide for tidal coupling to be responsible for the fast rotation rate, as is the case in genuine RS CVn systems.

Adopting $\Delta L \Delta M_2^{-1} A^{-1} V_c^{-1} \sim 0.06$, as read from Table 1, we use $R_2 = 10 R_\odot$ (see below), $r_g = 0.3$ (e.g. Tout & Hall 1991), $M_1 = 0.6 M_\odot$, $M_2 = 1.5 M_\odot$, $V_c = 16$ km s⁻¹, $v_{\text{rot},0} = 2$ km s⁻¹ in Eq. (19) and find that the spin up of HD 165141 requires a fraction $\Delta M_2/M_{2,0} = 0.008$ to be accreted to be consistent with its high current spin rate. The associated chemical pollution is consistent with that star displaying only mild chemical anomalies, since $\mathcal{F} = 0.011$ and $\log_{10} f = 0.3$ dex.

The reason why HD 165141 seems to be the only barium star exhibiting such a signature of spin accretion may be related to the fact that it is also the barium star with

the hottest (i.e. youngest) WD companion (having $T_{\text{eff}} \sim 35000$ K; Fekel et al. 1993). That situation contrasts with the other barium stars where the WD is usually not detected by the IUE satellite, indicating that it must be much cooler (i.e. older; see e.g. Böhm-Vitense et al. 1984). The cooling time scale of the WD companion of HD 165141 ($\tau_{\text{WD}} \sim 10^7$ y) is in fact shorter than the time spent by the present barium star as a giant, either on the first giant branch (assuming in this case that it is less massive than $\sim 2M_{\odot}$) or in the He clump. It may therefore be inferred that the mass transfer must have occurred when the barium star was already a giant star, contrary to the situation prevailing for the majority of barium stars that were formed as dwarfs (e.g. North & Duquennoy 1991; North, Berthet & Lanz 1994). For the dwarf stars, magnetic braking as well as the increase of moment of inertia accompanying the radius expansion on the giant branch will slow the rotation down (e.g. Habets & Zwaan 1989), thus erasing the possible spin up resulting from the accretion process. Magnetic braking is probably still operating in HD 165141, on a time scale of the order of 10^8 y if $v_{\text{rot}} \sim 14$ km s $^{-1}$ [see Eq. (2) of Habets & Zwaan 1989]. The slowing down of HD 165141 during the last 10^7 y, corresponding to the time τ_{WD} elapsed since the end of the mass transfer process, has thus been rather moderate, in agreement with the large observed spin velocity.

The current radius of $R_2 = 10 R_{\odot}$ adopted for HD 165141 in the above analysis corresponds to the lower limit derived from its 35 d photometric period and its $v \sin i = 14$ km s $^{-1}$ rotational velocity (Fekel et al. 1993). With such a radius and $T_{\text{eff}} \sim 4700 - 5000$ K, the star must currently be either in the core He-burning phase of evolution, or about midway on the RGB, according to the evolutionary tracks of Schaller et al. (1993). At the time of accretion (i.e. about 10^7 y ago, as given by the cooling time of the WD companion), the stellar radius may have been very different from its current value, being either much smaller (in the case that accretion occurred when HD 165141 was on the lower RGB, assuming it is still on the RGB now) or much larger (in the case that accretion occurred when HD 165141 was on the upper RGB, assuming that it reached its present core He-burning stage less than 10^7 y ago). It would be similar only in the case that HD 165141 remained in the core He-burning phase for the last 10^7 y (which is actually the most probable situation, as core He-burning lasts for at least 2.4×10^8 y in solar-metallicity stars of mass $2M_{\odot}$ or less). The fact that the stellar radius possibly varied in the course of stellar evolution following the accretion event, does not, however, invalidate the previous analysis based on Eq. (19), provided that the spin velocity before accretion, $v_{\text{rot},0}$, against which the current spin rate v is compared, is taken equal to the typical spin rate of normal stars in the *same* evolutionary phase, i.e. having the same current radius as HD 165141. In doing so, possible radius changes cancel out as they affect v and $v_{\text{rot},0}$ in the same way (provided that the accretion process did not alter the gyration radius r_g).

The possibility that *dwarf* barium stars have accreted spin angular momentum can be investigated on the sample studied by North & Duquennoy (1991) and North, Berthet & Lanz (1994). With the exception of one star (HD 198583), which has a rotational velocity substantially larger than F dwarfs of the same temperature, the other barium dwarfs seem to be rotating at rates comparable to normal (non-

barium) dwarfs. However, as in the case of barium giants, no WD companion could be detected for the barium dwarfs observed with IUE by North & Lanz (1991), implying ages $\geq 2 \times 10^8$ y. Since such ages are larger than the magnetic-braking time scale estimated above, the absence of fast rotators among dwarf barium stars is not at all unexpected. Ultraviolet data for HD 198583 would be of interest, in order to confirm our prediction of a correlation between fast rotation and the presence of a hot (i.e. young) WD companion.

6 SUMMARY

The SPH simulations presented in this paper model the accretion of the wind of a mass-losing star by its companion in the case where the wind velocity is comparable to the orbital velocity. The binary motion has then a strong influence on the accretion process, making analytic predictions based on the Bondi-Hoyle model suspect. In fact, we find that the mass accretion rate is at least ten times smaller than the rate predicted by the Bondi-Hoyle prescription, amounting to about 1% in a binary system with $M_1 = 3 M_{\odot}$, $M_2 = 1.5 M_{\odot}$, $A = 3$ AU and $v_{\text{wind}} = 15$ km s $^{-1}$ (in the case of an adiabatic gas with $\gamma = 1.5$). Smaller polytropic indices lead to slightly larger accretion rates of the order of 8%. These values probably represent upper limits, as the accretion rate decreases with increasing numerical resolution.

Despite the fact that the efficiency of wind accretion appears to have been overestimated in previous studies relying on the Bondi-Hoyle prescription, wind accretion still appears efficient enough to account for the chemical peculiarities exhibited by barium stars with orbital periods up to about 90 y.

The accretion of transverse linear momentum, controlling the eccentricity variation, appears to be negligible, at least in the present simulation involving a circular orbit.

Accretion of spin angular momentum is substantial, with a well-developed accretion disc forming in the isothermal case, contrary to a widespread belief that wind accretion cannot lead to the formation of such a disc. The spin up of the accreting star resulting from wind accretion may even be considered as an important diagnostic of this process. The mild barium star HD 165141 may be one case where such a spin up took place recently. Such fast-rotating post-mass transfer objects must be observed before the various braking processes (among which magnetic braking) slow the star down again. Therefore, we predict a correlation between WD temperature and barium star spin rate: fast spinning barium stars are predicted to have hot WD companions.

ACKNOWLEDGEMENTS

T.Theuns was supported by the EEC Human Capital and Mobility Programme under contract CT941463.

REFERENCES

- Benz W., 1989, in Buchler J.R., ed., Numerical Modeling of Stellar Pulsations. Kluwer, Dordrecht, p. 269
- Boffin H.M.J., Cerf N., Paulus G., 1993, A&A, 271, 125
- Boffin H.M.J., Jorissen A., 1988, A&A, 205, 155

Boffin H.M.J., Začs L., 1994, *A&A*, 291, 811
 Böhm-Vitense E., Nemeč J., Proffitt Ch., 1984, *ApJ*, 278, 726
 Bondi H., 1952, *MNRAS*, 114, 195
 Bondi H., Hoyle F., 1944, *MNRAS*, 104, 273
 Bowen G.H., 1988, *ApJ*, 329, 299
 de Medeiros J.R., Mayor M., Simon Th., 1992, *A&A*, 254, L36
 Fekel F.C., Henry G.W., Busby M.R., Eitter J.J., 1993, *AJ*, 106, 2370
 Gingold R.A., Monaghan J.J., 1977, *MNRAS*, 181, 375
 Griffin R.F., 1991, *The Observatory*, 111, 29
 Groenewegen M.A.T., de Jong T., 1993, *A&A*, 267, 410
 Habets G.M.H.J., Zwaan C., 1989, *A&A*, 211, 56
 Han Z., Eggleton P.P., Podsiadlowski P., Tout C.A., 1995, *MNRAS*, in press
 Hoyle F., Lyttleton R.A., 1939, *Proc. Cam. Phil. Soc.*, 35, 405
 Huang S.S., 1956, *AJ*, 61, 49
 Hunt R., 1971, *MNRAS*, 154, 141
 Jorissen A., Boffin H.M.J., 1992, in Duquennoy A., Mayor M., eds., *Binaries as tracers of stellar formation*. Cambridge Univ. Press, Cambridge, p. 110
 Jorissen A., Hennen O., Mayor M., Bruch A., Sterken Ch., 1995a, *A&A* 301, 707
 Jorissen A., Schmitt J.H.M.M., Carquillat J.M., Ginestet N., Bickert K.F., 1995b, *A&A*, in press
 Lambert D.L., 1985, in Jaschek M., Keenan P.C., eds., *Cool Stars with Excesses of Heavy Elements*. Reidel, Dordrecht, p. 191
 Lucy L.B., 1977, *AJ*, 82, 1013
 Matsuda T., Inoue M., Sawada K., 1987, *MNRAS*, 226, 785
 Matsuda T., Ishii T., Sekino N., Sawada K., Shima E., Livio M., Anzer U., 1992, *MNRAS*, 255, 183
 McClure R.D., Woodsworth A.W., 1990, *ApJ*, 352, 709
 Meyer, F., Meyer-Hofmeister, H., 1979, *A&A*, 78, 167
 North P., Duquennoy A., 1991, *A&A*, 244, 335
 North P., Lanz T., 1991, *A&A*, 251, 489
 North P., Berthet S., Lanz T., 1994, *A&A*, 281, 775
 Nussbaumer H., Stencel R.E., 1987, in Kondo Y., de Jaeger C., Linsky J.L., eds., *Exploring the Universe with the IUE satellite*. Kluwer, Dordrecht, p. 203
 Packett W., 1981, *A&A*, 102, 17
 Proffitt C.R., 1989, *ApJ*, 338, 990
 Proffitt C.R., Michaud G., 1989, *ApJ*, 345, 998
 Ruffert M., 1994, *ApJ*, 427, 342
 Ruffert M., Arnett D., 1994, *ApJ*, 427, 351
 Theuns T., David, M., 1992, *ApJ*, 384, 587
 Theuns T., Jorissen A., 1993, *MNRAS*, 265, 946 (Paper I)
 Schaller G., Schaerer D., Meynet G., Maeder A., 1993, *A&AS* 96, 269
 Sørensen S., Matsuda T., Sakurai T., 1975, *Ap&SS*, 33, 465
 Tout C.A., Eggleton P.P., 1988, *MNRAS*, 231, 823
 Tout C.A., Hall D.S., 1991, *MNRAS*, 253, 9
 Utsumi K., 1985, in Jaschek M., Keenan P.C., eds., *Cool Stars with Excesses of Heavy Elements*. Reidel, Dordrecht, p.243
 Weidemann V., 1984, *A&A*, 134, L1
 Waters L.B.F.M., Trams N.R., Waelkens C., 1992, *A&A*, 262, L37
 Začs L., 1994, *A&A*, 283, 937

APPENDIX

Following the method of Huang (1956) we derive expressions for the change in orbital parameters due to accretion and the action of gravitational forces. Assuming that star 1 suffers a spherically symmetric mass loss, then conservation of linear momentum in a small interval of time ∂t can be written as:

$$\mathbf{G}_1 \partial t = [(M_1 + \partial M_1)(\mathbf{v}_1 + \partial \mathbf{v}_1) - \partial M_1 \mathbf{v}_1]$$

$$- [M_1 \mathbf{v}_1] \quad (21)$$

$$\begin{aligned} \mathbf{G}_2 \partial t &= [(M_2 + \partial M_2)(\mathbf{v}_2 + \partial \mathbf{v}_2)] \\ &- [M_2 \mathbf{v}_2 + \sum_w \partial m_w \mathbf{v}_w], \end{aligned} \quad (22)$$

where the \mathbf{G} 's refer to the gravitational force exerted by the wind on the corresponding star and $\sum_w \partial m_w \mathbf{v}_w$ denotes the change in momentum of the accreting star due to momentum accreted from the wind. The change in orbital parameters A , P and e follows from the change in mass, energy E and angular momentum h per unit reduced mass through:

$$\partial A/A = \partial(M_1 + M_2)/(M_1 + M_2) - \partial E/E \quad (23)$$

$$\partial P/P = \partial(M_1 + M_2)/(M_1 + M_2) - \frac{3}{2} \partial E/E \quad (24)$$

$$\begin{aligned} e \partial e / (1 - e^2) &= \partial(M_1 + M_2)/(M_1 + M_2) - \frac{1}{2} \partial E/E \\ &- \partial h/h, \end{aligned} \quad (25)$$

where $E = v_t^2/2 + v_r^2/2 - (M_1 + M_2)/r$ and $h = r v_t$, with r , $v_r (= \dot{r})$ and v_t being respectively the radius vector, the radial velocity and the transverse velocity of the accreting star in the relative frame where the mass-losing star is at rest. Denoting by $v_{1,y}$ and $v_{2,y}$ the projections of the individual (inertial) velocities on the y direction transverse to the radius vector and oriented along the orbital motion of star 1, one has $v_t = v_{1,y} - v_{2,y}$. Orbit-averaged variations, denoted by $\langle \rangle$, can be computed from the change in the relative transverse velocity ∂v_t , obtained from Eqs. (21) and (22):

$$\begin{aligned} \partial v_t &= \partial v_{1,y} - \partial v_{2,y} \\ &\equiv -F_y \partial t / M_2 \\ &= G_{1,y} \partial t / M_1 - G_{2,y} \partial t / M_2 \\ &- \sum_w \partial m_w (v_{w,y} - v_{2,y}) / M_2. \end{aligned} \quad (26)$$

Here, as before, $G_{1,y}$ and $G_{2,y}$ are the projections of the gravitational forces on the transverse direction. With the above conventions, $G_{1,y}$ and $G_{2,y}$ are positive, since gas is lagging behind the accretor with respect to its orbital motion. Hence, the mass-losing star is accelerated by that material whereas the accretor is decelerated. Note that ∂v_t refers to the variation of v_t induced by the mass transfer (and not to the variation along the orbit due to keplerian motion).

When computing the orbit averages $\langle \partial E \rangle$ and $\langle \partial h \rangle$, it is assumed that the mass accretion rate \dot{M}_2 and the force F_y do not depend on the phase of the binary. Clearly, this assumption will be poor when the eccentricity is large, so that the relations derived here are only valid for systems with small eccentricities. It should also be noted that keeping the force F_y constant along the orbit is not equivalent to Huang's parametrization in terms of constant $\lambda = -\partial(M_2 v_t)/V_c \partial M_2 = -v_t/V_c + F_y \partial t / V_c \partial M_2$. Indeed, λ and F_y cannot both remain constant along an eccentric orbit, since v_t/V_c varies with orbital phase in an eccentric orbit. Therefore, the relations derived here are not equivalent to Huang's.

Averaging over the orbital period then amounts to using the following mean values:

$$\langle \dot{r} \rangle = 0 \quad (27)$$

$$\langle \dot{r}^2 \rangle = V_c^2 (1 - (1 - e^2)^{1/2}) \quad (28)$$

$$\langle r \rangle = A(1 + e^2/2) \quad (29)$$

$$\langle 1/r \rangle = 1/A \quad (30)$$

$$\langle 1/r^2 \rangle = 1/[A^2(1 - e^2)^{1/2}]. \quad (31)$$

As an example of how the calculation is done, we will compute the orbit-averaged change in kinetic energy per unit mass, $T = \frac{1}{2} v_t^2 + \frac{1}{2} \dot{r}^2$. Assuming F_y (i.e. ∂v_t) constant along the orbit, the orbit-averaged differential of the first term in T writes:

$$\begin{aligned} \langle v_t \partial v_t \rangle &= \langle v_t \rangle \partial v_t \\ &= -\frac{h}{A} \frac{F_y \partial t}{M_2} \end{aligned} \quad (32)$$

where we used the average $\langle v_t \rangle = h \langle 1/r \rangle = h/A$.

Analogously, we obtain for the second term:

$$\begin{aligned} \langle \dot{r} \partial \dot{r} \rangle &= \langle \dot{r} \partial \left(\frac{M_2 \dot{r}}{M_2} \right) \rangle \\ &= \langle \dot{r} \frac{\partial(M_2 \dot{r})}{M_2} - \dot{r}^2 \frac{\partial M_2}{M_2} \rangle \\ &= \langle \dot{r} \rangle \frac{\partial(M_2 \dot{r})}{M_2} - \langle \dot{r}^2 \rangle \frac{\partial M_2}{M_2} \\ &= -V_c^2 (1 - (1 - e^2)^{1/2}) \frac{\partial M_2}{M_2} \end{aligned} \quad (33)$$

where we assumed $\partial(M_2 \dot{r})$ to be constant over an orbital period and used the averages in Eqs. (27–28). The sum of these last two results gives $\langle \partial T \rangle$.

Proceeding in the same spirit, we get

$$\frac{\langle \partial \Omega \rangle}{E} = 2 \frac{\partial M_1 + \partial M_2}{M_1 + M_2} \quad (34)$$

$$\frac{\langle \partial h \rangle}{h} = -\frac{(1 + e^2/2) F_y \partial t}{(1 - e^2)^{1/2} V_c M_2} \quad (35)$$

where Ω denotes the potential energy per unit mass. Using these orbital averages in Eqs. (23–25) then leads to Eqs. (13–15) at order e^2 .

The change in eccentricity given by Eq. (25) can be understood intuitively as follows: first recall that, for a given energy, the circular orbit has the maximum angular momentum. It follows that increasing the angular momentum $\partial h > 0$ while keeping masses and energy constant, decreases the eccentricity, hence circularising the binary. Increasing the energy $\partial E > 0$, while keeping h constant, has the opposite tendency.